

# MAVNet: an Effective Semantic Segmentation Micro-Network for MAV-based Tasks

Ty Nguyen<sup>1</sup>, Tolga Özaslan<sup>1</sup>, Ian D. Miller<sup>1</sup>, James Keller<sup>1</sup>, Shreyas Shivakumar<sup>1</sup>, Giuseppe Loianno<sup>2</sup>, Camillo J. Taylor<sup>1</sup>, Vijay Kumar<sup>1</sup>, Joseph H. Harwood<sup>3</sup>, Jennifer Wozencraft<sup>3</sup>

**Abstract**—Real-time image semantic segmentation is an essential capability to enhance robot autonomy and improve human situational awareness. In this paper, we present MAVNet, a novel deep neural network approach for semantic segmentation suitable for small scale Micro Aerial Vehicles (MAVs). Our approach is compatible with the size, weight, and power (SWaP) constraints typical of small scale MAVs, which can only employ small processing units and GPUs. These units have typically limited computational capacity, which has to be concurrently shared with other real time performance tasks such as visual odometry and path planning. Our proposed solution MAVNet, is a fast and compact network inspired by ERFNet [1] and features  $\sim 400$  times fewer parameters in comparison. Experimental results on multiple datasets validate our proposed approach. Additionally, comparisons with other state of the art approaches show that our solution outperforms theirs in terms of speed and accuracy achieving up to 48 FPS on an NVIDIA 1080Ti and 9 FPS on the NVIDIA Jetson Xavier when processing high resolution imagery. Our algorithm and datasets are made publicly available.

## I. INTRODUCTION

Micro Aerial Vehicles (MAVs) equipped with on-board sensors and computers can be a viable and inexpensive solution for assisting humans in complex, labor-intensive, high-cost tasks. They can even replace humans in tasks dangerous to accomplish manually [2]. A typical example is the periodic inspection and maintenance of critical infrastructure such as dams, penstocks, and locks [3]. These are critically important tasks required to prevent possible catastrophic structural failures. Fast and autonomous inspection with MAVs would help enable the automation of the inspection process while lowering the cost, providing information about areas inaccessible to a human worker, and preventing occupational accidents.

This work was supported by the MAST Collaborative Technology Alliance - Contract No. W911NF-08-2-0004, ARL grant W911NF-08-2-0004, ONR grants N00014-07-1-0829, N00014-14-1-0510, ARO grant W911NF-13-1-0350, NSF grants IIS-1426840, IIS-1138847, DARPA grants HR001151626, HR0011516850, and supported in part by the Semiconductor Research Corporation (SRC) and DARPA.

T. Özaslan acknowledges the fellowship from The Republic of Turkey Ministry of National Education.

<sup>1</sup> The authors are with the GRASP Lab, University of Pennsylvania, Philadelphia, PA 19104 USA. email: {tynguyen, ozaslan, iandm, jfkeller, sshreyas, cjtaylor, kumar}@seas.upenn.edu

<sup>2</sup> The author is with the New York University, Tandon School of Engineering, 6 MetroTech Center, 11201 Brooklyn NY, USA. email: {loiannog}@nyu.edu.

<sup>3</sup> The authors are with the United States Army Corps of Engineers, Washington, DC 20314 USA. email: {joseph.h.harwood, jennifer.m.wozencraft}@usace.army.mil



Fig. 1: The MAV platform flying inside a penstock at Center Hill Dam, TN. The robot collects images from four on-board cameras with the only illumination source being the on-board power LEDs.

In this context, the ability to perform real-time semantic segmentation is crucial for field robots to enhance their autonomy and decision making processes. In the field of semantic segmentation, deep learning has become the *de-facto* approach with superior accuracy and robustness over the classical machine learning approaches [4], [5]. The most prominent among many application areas are agricultural inspection for fruit counting [6] and disease detection [7], vehicle and pedestrian traffic monitoring [8], [9], and structural health monitoring of critical infrastructure [10], [11], [12] to name a few.

Conventionally, deep learning approaches require significant computational power. Since the introduction of residual networks such as ResNet [13] which add increasing numbers of layers to the network, there has been much emphasis on accuracy over compactness and efficiency of algorithms. While outsourcing the data to the cloud is a solution often chosen when on-board computation is limited, it inhibits the robot's operations in remote areas or subterranean regions where wireless connectivity is often not available. For robotic applications, it is often desirable to perform image segmentation at high speed on-board the platform. This is particularly challenging for robots such as small scale MAVs, which are subject to size, weight, and power (SWaP) constraints. Examples of such applications include relative visual localization of other robots in multi-robot systems [14], semantic mapping [15], and damage detection for infrastructure inspection [16], [17]. Semantic image segmentation is a key enabler of high level robotic perception, and is therefore a necessary prerequisite for greater levels of autonomy. MAVs are representative target platforms, as their flexibility makes them ideal for tasks such as inspection and monitoring, but their SWaP constraints severely limit the on-

board computational capabilities.

There are some recent research in deep learning inference at the edge [18], [1]. However, most of these works focus on datasets collected from ground vehicles, which lack the challenges presented with MAV imagery. Images from MAVs can often be in low or dynamically illuminated environments, with moving objects, and in presence of image noise as in this work. Thus, these solutions cannot be applied directly to such scenarios.

In this work, we present MAVNet, a novel deep neural network architecture for image segmentation at high speed on resource constrained platforms. We evaluate our approach on datasets collected from a penstock shown in Fig. 1 for detection of critical areas, and on another dataset for in-flight multi-MAV segmentation. Our method shows competitive performance with current state-of-the-art approaches, while running at practically feasible frame rates, 48 FPS on NVIDIA 1080Ti and 9 on NVIDIA Jetson Xavier with low memory utilization on high resolution ( $1280 \times 1024$ ) imagery.

Currently, most evaluation is performed on datasets like KITTI [19] or CityScapes [20], which are useful for vehicle autonomy, but are unrepresentative of the challenging environments encountered by MAVs. Our approach provides an effective solution for segmenting critical areas in challenging environments such as dam penstocks. Penstocks are large, approximately 5m diameter steel or concrete tunnels which deliver water from reservoirs to turbines in hydroelectric dams. These tunnels can be hundreds of meters long, almost completely featureless, have no external illumination, are extremely dusty, and require regular maintenance and inspection.

Similarly, we show that a fast and effective segmentation scheme can also be used for other MAV relevant tasks such as detection of moving objects such as other MAVs, proving its practical applicability. This application is equally challenging as in-flight MAVs are moving fast and appear in a wide variety of angles and distances, making the detection problem equally challenging.

Our primary contributions are as follows. *First*, we present a novel deep learning network for achieving high speed image segmentation at full resolution with minimal resources and computational demands. *Second*, we evaluate the network on two different, challenging datasets, demonstrating the flexibility of our approach as well as performance improvements over the current state-of-the-art. *Third*, we make the datasets publicly available in order to encourage further work in developing algorithms for highly challenging environments.

## II. RELATED WORK

### A. Real-Time Deep Learning

State-of-the-art segmentation algorithms such as ResNet [13] and VGG [21] have shown excellent performance on a variety of different datasets. However, these are highly complex networks, involving many layers, and require large amounts of computational capability for inference at high

speed. In [22], the authors present ENet, which can run at up to 7 fps on a Jetson TX1, but at the cost of significant downsampling. ErfNet [1] builds on ENet, achieving superior accuracy by using a more complex but slightly slower architecture. The authors of MobileNet [23] develop an architecture with several hyperparameters allowing the user to tune their model for particular constraints required by the application. ESPNet [24] uses efficient spatial pyramids to achieve accuracy close to ResNet but at higher inference speeds. The authors of ICNet [25] report that they significantly outperform ENet on CityScapes while running at 30fps with  $1024 \times 2048$  resolution, but this performance is limited to desktop grade computational platforms such as a Titan X GPU. The authors do not test their algorithm on embedded devices such as the Jetson.

While these methods have achieved accurate results at reasonably high inference rates on a large number of classes, validation for all of these methods is typically performed on driving datasets such as KITTI or Cityscapes. To our knowledge, we are the first to benchmark and evaluate existing networks on challenging datasets such as penstocks and visual MAV detection, while designing and evaluating a novel network architecture explicitly designed for high resolution real-time semantic segmentation with fewer target classes.

### B. Deep Learning for Visual Infrastructure Inspection

There has been significant interest in using deep learning techniques for infrastructure inspection. In a recent study, [10] introduces a sliding-window technique using a CNN-based classifier to detect cracks on concrete and steel surfaces. The major drawback of this method is that it cannot satisfy real-time processing requirements and would fail in detecting small defects which are very frequent in our images. This type of framework is also not data-efficient since it processes an image patch as a single sample.

[26] uses CNNs to detect defects on different types of materials such as fabric, stone and wood. They compare their network to conventional machine learning methods such as the Gabor Filter, Random Forest and Independent Component Analysis. However, the authors do not present a complete system for autonomous data collection and automated defect detection, and do not optimize the inference speed of their classifier.

In a similar application to ours, [12] propose to feed a CNN with low-level features such as edges so as to obtain a mixture of low and high level features before classifying pixels to detect defects on concrete tunnel surfaces. Unlike this work, we propose an end-to-end fully convolutional neural network that does not depend on handcrafted features and also works with arbitrary input image sizes. Indeed, some of the low-level features used in their work are neither easy to obtain nor provide useful information for the CNN such as edges, texture and frequency. This is due to the characteristics of the noise caused by dust and mist as well as the complex appearance of the penstock surface.

In general, to the best of our knowledge, this work is the first attempt to consider the use of deep learning techniques for infrastructure inspection on a computationally constrained platform.

### III. DATASETS

In this study, we evaluate the performance of deep network models on two different datasets that we collected using autonomous MAVs.

#### A. Penstock Dataset

1) *Data Collection*: The first dataset provided in this study is collected with a customized DJI-F550 MAV described in [27] that autonomously flies inside a penstock at Center Hill Dam, TN. Sample images and corresponding labels are shown in Fig. 2a. Images are partially occluded: bottom-facing cameras by the landing gear, and top-facing by the propellers. Images also have systematic uneven brightness due to reflections from wet surfaces and limited illumination from the on-board LEDs. The pink labels on the image represent corroded regions of the penstock surface. There are four fish-eye cameras mounted on the robot such that the combined field of view covers the annulus of the tunnel. We provide two sequences of images taken from two flights with different lighting conditions, one for training and the other for testing. We label every 20<sup>th</sup> frame in each sequence. We then only use images captured from the two cameras on the left of the first sequence for training and those taken from two cameras on the right of the second sequence for testing. This way, no part of the penstock seen in training is seen by the classifier when testing.

2) *Data Preprocessing*: Weak on-board illumination, reflective wet surfaces, and noise due to dust and mist particles cause images to be either dark and textureless or very bright and occluded with bright dust traces (Fig. 2). Hence, we preprocess the images to suppress these effects before feeding them into our network. We apply limited adaptive histogram equalization using OpenCV’s CLAHE module to mitigate the brightness imbalance. Also, image regions occluded by the MAV’s landing gear, camera lens covers, and propellers are masked out. We choose to perform inference on the original distorted images, as it is then easy to post-process the segmentation to undistort or project onto the desired visualization.

We use 4 classes to label pixels in each training image. These classes are :normal coating, corrosion, rivet and water. In order to improve confidence in labeling, each training image is labeled by *three* humans separately.

#### B. Drone Dataset

The second dataset (Fig. 2b) is a multi-robot flying dataset collected indoors, whose primary purpose is to train real-time vision guided MAV tracking systems. This dataset is collected from on-board three of our custom Falcon 250 MAV platforms, each equipped with an Open Vision Computer sensor-compute package [28]. The images are acquired from the on-board gray-scale Python 1300 cameras. This

is a challenging dataset as the relative motion between the drones is constantly changing, resulting in large variance in size of the target object with respect to the backgrounds. We collect pixelwise labels for 110 images used for training and 46 used for testing. This dataset is similar to the penstock dataset in the sense that the fraction of pixels in the regions of interest, i.e MAV pixels, to the background pixels is small and is therefore challenging for semantic segmentation networks that trade coarse level segmentation for real-time performance.

### IV. NETWORK DESIGN

Unlike common state-of-the art deep network models benchmarked on large datasets such as Cityscapes and MS COCO, networks intended for robotic vision tasks run on on-board processors and must therefore satisfy performance, computational, and memory constraints. As we will demonstrate in our experiments and others have observed [1], it is insufficient to merely reduce the number of parameters in a more complex network, particularly without making significant performance sacrifices. We therefore believe that designing a new network structure, rather than attempting to re-scale existing ones, is necessary. Inspired by ErfNet [1], this section details the intuitions and experiments that lead to our proposed network design.

#### A. Downsampling

Despite downsampling presenting undesired side-effects such as spatial information loss and potential checkerboard artifacts introduced during upsampling to the original image size, it is still a widely preferred pre-processing step due to its various benefits. Downsampling can help reduce spatial redundancy, making the precedent filtering layers operate with lower resolution features and thereby saving significant computational and memory cost. Additionally, filtering using reduced input features results in features with a larger receptive field, allowing them to gather broader context. This capability is essential to classifying objects with significant variation in size.

A simple trick to mitigate the first side effect of downsampling — spatial information loss — is to increase the number of output features by two before downsampling by two, for example. FCN [29] and UNet [30] go a step further and utilize skip connections from early layers of the encoder to the decoder to preserve spatial information. However, these long skip connections require large amounts of memory to store the intermediate results for later use, slowing down the overall inference time. SegNet [31] and ENet [22] solve this problem when reversing the downsampling by storing the elements chosen in max pooling when doing downsampling.

We investigate the effect of downsampling by evaluating two variants of ERFNet: one using downsampling and one without downsampling on our two datasets. Results show that the version without downsampling does not perform significantly better than the other at the price of an increased time and memory.

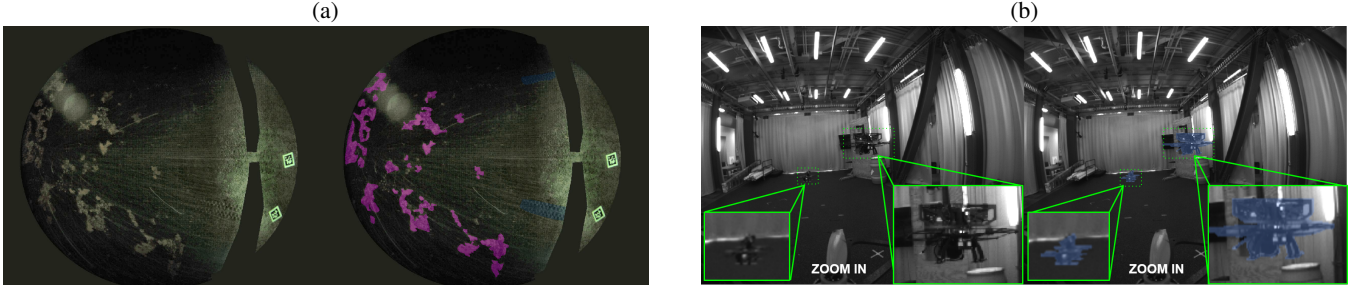


Fig. 2: (a) A sample image captured by one of the fish-eye cameras from the penstock dataset. From left to right: input image, labeled image. Pink: corrosion, light blue: rivet; (b) A sample image from the drone dataset. From left to right: input image, labeled image. Light blue: drone

We also study different downsampling blocks. We find that the downsampler block used in In [1] results in inferior performance compared to conv-conv-pool in [32] when the number of layers and number of features of the network are significantly shrunk. Thus, we make use of two conv-conv-pool blocks to downsample the input image as the first two blocks of our network.

### B. Dilated Convolution

Dilated convolution or atrous convolution is an effective and inexpensive way to increase the receptive field of a network as demonstrated in successive works such as [1], [33]. By stacking multiple dilated convolution layers with a dilation rate larger than one, the precedent features can achieve an exponential increase in receptive field with the same amount of parameters and computation as regular convolution does. A larger receptive field arguably allows the network to see not only the object but also the context in which the object stands which can be leveraged to improve the segmentation performance. However, unlike ErfNet, we find that stacking more than  $K$  dilated convolutions with dilation rate of 2 (where  $2^K$  is equal to input image size) is unnecessary as the precedent dilated convolutions have no effect. This observation helps remove a significant amount of dilated convolution from ErfNet.

### C. Depth-wise Feature Aggregation Block (DWFab)

The backbone of our MAVNet is a simple but effective depth-wise feature aggregation block (DWFab). As shown in Fig. 3, DWFab blocks differ from non-bottleneck in two ways. First, DWFab blocks make use of depth-wise separable convolutions instead of regular convolutions for  $3 \times 1$  and  $1 \times 3$  convolutions. These depth-wise separable convolutions can effectively reduce computational cost and also enable the use of larger spatial filter sizes at low cost.

Secondly, after going through two depth-wise separable convolutions, the output is concatenated with the original input, followed by a  $1 \times 1$  convolution to achieve the desirable number of output features.

This design provide more flexibility than the addition operation in the original non-bottleneck block. With an addition operation, the input features are forced to linearly interact with the output features. This design, however, allows the

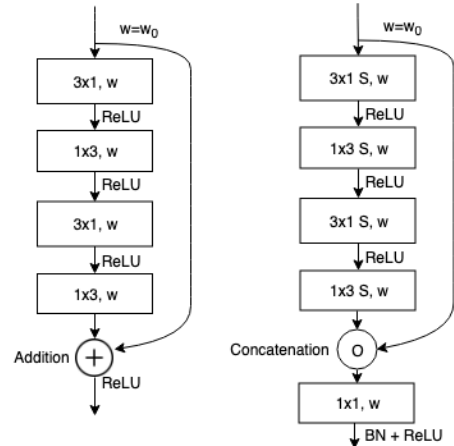


Fig. 3: Non-bottleneck v.s. Depth-wise Feature Aggregation Blocks. S stands for depth-wise separable convolution

network to determine itself how the two sources of features interact.

In addition, the upsampler module in ERFNet is replaced by nearest-neighbor upsampling followed by a  $1 \times 1$  convolution since we find that transposed convolution causes the checkerboard issue.

We also investigate the max-pooling function and find that it is significantly inferior to both addition and concat-conv. Our complete FCB block is shown in Fig. 3.

### D. Network Architecture

As can be seen in Fig. 4, our network is quite simple compared to ErfNet. The encoder part consists of two Conv-Conv-Pool blocks, followed by four DWFab blocks that have dilation rates of 2, 4, 8, 16 respectively.

Followed by these blocks is a decoder which consists of two upsampling blocks with a non-bottleneck, as used in ErfNet, in between and a  $1 \times 1$  convolution at the end to output the logits. A short decoder is used for two reasons. First, it can reduce computation as well as eliminate the need of skip connections, since the whole network is short. Secondly, in most MAV-based tasks such as inspection and tracking, misclassifying an object as non-object has much more cost than misclassifying a non-object as object. Therefore, an

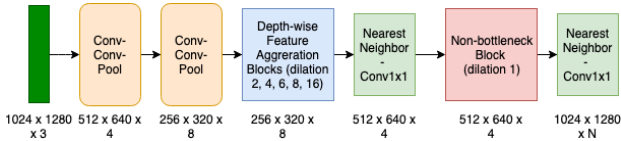


Fig. 4: Network Architecture. Input used in this study is of size  $1024 \times 1280 \times 3$  and the output segmentation is  $1024 \times 1280 \times N$ , with  $N$  is the number of classes.

algorithm that delivers more false positives than negatives is preferable to one that does the opposite. We empirically find that a short decoder provides a better false rate than a long decoder. Section VII-B details this observation.

We additionally replace the upsampler module in ErfNet by a simple upsampling block which consists of a nearest neighbor upsampling followed by a  $1 \times 1$  convolution, as the transposed convolution used in the last layers of ErfNet causes the checkerboard issue when we shrink down the network size.

To demonstrate the effectiveness of the DWFab block, in the following sections, we carry out experiments to compare MAVNet with UNet, ENet, and ErfNet. In addition, we create a variant of ErfNet with the same number of blocks as MAVNet, except the first two downsampling blocks are replaced by a downsampler, and the DWFab blocks are replaced by non-bottleneck blocks as in ErfNet. This network is referred as S-ErfNet for the remainder of this paper.

## V. TRAINING

### A. Focal Loss for Multi-class Classification

The problem of class imbalance often appears when performing multi-class segmentation. In robotics and medical imaging applications, this problem is exacerbated since the training data set is often small due to the expensive data acquisition process.

To mitigate this problem, we make use of the focal loss, introduced in [34]. We can generalize focal loss [34] for the multi-class classification problem as follows:

$$\mathbf{L}_{Focal} = -\frac{1}{N} \sum_{n=1}^N \sum_{c=1}^C (1 - \hat{y}_{nc})^\gamma y_{nc} \log \hat{y}_{nc}, \quad (1)$$

where  $\gamma > 0$  is a tunable parameter. The effect of the focal loss and  $\gamma$  value can be understood in the following manner: When a difficult sample is misclassified, with the true class given low confidence ( $\hat{y}_{nc}$  is small), the weighting factor becomes close to 1, preserving that sample's contributions to the total loss. In contrast, an easy sample correctly classified with a high confidence value,  $\hat{y}_{nc}$ , will have its weight close to 0, reducing its contribution to the total loss. In summary, the focal loss function can appreciate the weighting of difficult samples, regardless of which class they belong to, by giving more them more weight and depreciating easy samples. In our experiments, we set  $\gamma = 2$  as recommended by the authors. Since the drone dataset has a large unbalance between positive samples (drone pixels) and negative samples (non-drone pixels), we introduce additional weights for each sample type in the loss: 20 for the drone and 1 for not-drone.

### B. Training Scheme

All the deep network models investigated in this study are implemented in Tensorflow [35]. The training procedure is the same with all models: use mini-batch gradient descent with the batch-size of 4, Adam Optimizer [36] with  $\beta_1 = 0.9$ ,  $\beta_2 = 0.999$  and  $\varepsilon = 10^{-8}$ , learning rate 0.001. All models are trained for 30,000 iterations or until divergence. Online data augmentation is used including random rotation, random cropping and padding, random gamma shifting, random brightness shifting, and random color shifting. Our implementation is publicly available at <https://github.com/tynguyen/MAVNet>.

## VI. BENCHMARKS

We benchmark our proposed network in comparison with networks including UNet, ErfNet, ENet and S-ErfNet on both the penstock and drone datasets. The performance is evaluated using three metrics.

### A. Metrics

For each model, we report three metrics commonly used in semantic segmentation: Intersection over union (IoU), false rate, and accuracy.

$$\text{IoU} = \frac{TP}{TP + FP + FN}, \quad (2)$$

$$\text{False Rate} = \frac{FN}{FN + TN}, \quad (3)$$

$$\text{Accuracy} = \frac{TP + TN}{TP + FP + TN + FN}, \quad (4)$$

where  $TP$  = Pixels correctly classified as the object in the ground truth and by algorithm;  $FP$  = Pixels not classified as the object in the ground truth, but classified as the object by algorithm;  $TN$  = Pixels not classified as the object in ground truth and by algorithm;  $FN$  = Pixels classified as object in ground truth, but not classified as object by algorithm. Obtaining a segmentation model with high IoU, small false rate and high accuracy is desirable, but often infeasible to achieve in practice. Instead, there is often a trade-off between these metrics when selecting a model. For example, in inspection and tracking systems, a small *false rate* is often chosen along with decent IoU and accuracy values.

### B. Penstock Dataset

Tab. I details the three metrics for each class on the penstock dataset.

As can be seen, performance of each model varies with respect to different class of objects. For example, UNet and ENet perform well on corrosion and water, but poorly on rivets, while ErfNet performs decently on both classes. MAVNet, on the other hand, has a comparable IoU with UNet while having lowest false rate on corrosion. It also tops the two best in IoU measurement of rivet detection. Overall, MAVNet has highest average IoU over all classes.

	Corrosion			Rivet			Water			Mean IoU
	IoU	False rate	Accuracy	IoU	False rate	Accuracy	IoU	False rate	Accuracy	
UNet	33.17	3.04	93.94	3.13	2.96	97.04	84.38	0.82	99.18	26.87
ErfNet	27.95	6.02	92.25	32.14	1.27	98.40	25.88	0.88	98.99	32.53
ENet	17.34	12.25	87.66	9.26	2.55	97.36	53.13	0.32	99.67	30.20
S-ErfNet	25.38	3.90	87.51	23.2	1.44	97.50	0.05	0.6	98.07	22.28
MAVNet	29.92	<b>1.30</b>	86.54	30.23	1.65	97.92	3.91	0.81	98.96	<b>33.16</b>

TABLE I: Class-wise performance of MAVNet in comparison with other methods on penstock dataset. All metrics are in %

Items	UNet	ErfNet	ENet	S-ErfNet	MAVNet
IoU (%)	44.29	42.04	43.09	35.52	39.23
False rate (%)	0.02	0.03	0.04	0.01	0.005
Accuracy (%)	99.92	99.87	99.91	99.84	99.82

TABLE II: Performance comparison on drone detection dataset.

### C. Drone Detection Dataset

Table II details the three metrics for each class on the drone dataset. These tables also show the advantage of MAVNet in *false rate* as MAVNet yields the lowest number. This small *false rate* is essential for tracking systems to avoid missing tracked objects. MAVNet also yields comparable accuracy and IoU.

## VII. PERFORMANCE ANALYSIS

### A. Speed and Performance Tradeoff

In this section, we report the performance of models with respect to inference speed and their model’s complexity. Details are given in Tab. III, where performance in IoU is the average IoU of every class on each dataset. Mean IoU 1 is the average IoU of *corrosion*, *rivet*, *water* on penstock dataset and mean IoU 2 is just IoU of *drone* on the drone dataset.

MAVNet is by far more compact than UNet, ErfNet and ENet as it has  $\sim 1500$  times less parameters than UNet and  $\sim 400$  times less than ErfNet, making it perfectly suitable for embedded systems.

To measure the speed, we run the pretrained models and report the inference speed of models on the NVIDIA Jetson Xavier, an embedded platform often used for small robots such as MAVs. Speed is measured for input image of size  $1024 \times 1280 \times 3$  and batch size of 1.

Fig. 5 and 6 visualize the corresponding inference speed and performance of each model in each dataset. Note that all models are trained from scratch for each dataset with the same training scheme. These two figures show the effectiveness of our network design. As can be seen in Fig. 5, MAVNet has a comparable speed with S-ErfNet while significantly outperforming it, and even slightly outperforming the unmodified ErfNet which is much slower. MAVNet is similarly superior to other methods.

Fig. 6 demonstrates MAVNet’s flexibility, yielding similar results for a very different dataset. It still outperforms S-ErfNet while having slightly lower IoU than that of UNet and ErfNet, which run 4–7 times slower than it does.

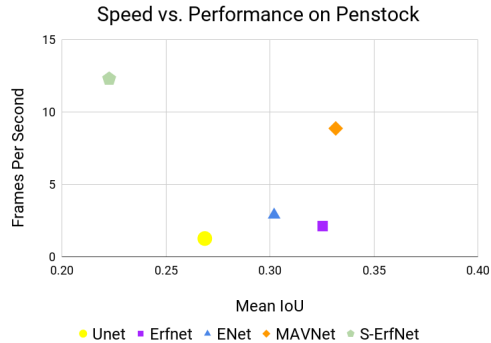


Fig. 5: Speed v.s. mean IoU over 3 object classes on penstock dataset. MAVNet outperforms other methods and achieves a decent speed compared to S-ErfNet. Running time is measured on NVIDIA Xavier.

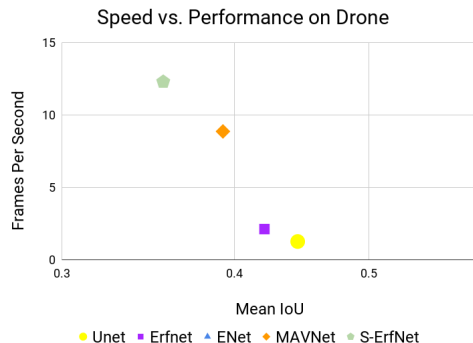


Fig. 6: Speed v.s. mean IoU over 3 object classes on drone dataset. MAVNet outperforms other methods and achieves a decent speed compared to S-ErfNet. Running time is measured on NVIDIA Xavier.

### B. Qualitative Results

Fig. 7 depicts a case where MAVNet outperforms other methods qualitatively. Compared to other methods, the result from MAVNet retains most of the details in the image, including the rivets. ErfNet fails in this case while ENet does a similarly poor job in corrosion detection but completely fails to detect the rivets. S-ErfNet yields many more false positives than MAVNet does.

Fig. 8 shows a case where both ErfNet and its simplified variant yield large regions of false positive. MAVNet, on the other hand, can provide a comparable result to UNet and ENet.

In our network design, we emphasize our short decoder for increasing speed and lowering the false rate. A drawback

Items	UNet	ErfNet	ENet	S-ErfNet	MAVNet
Mean IoU 1 (%)	26.87	32.53	30.20	22.28	33.16
Mean IoU 2 (%)	44.43	42.04	44.07	35.52	39.23
Time (ms)	785	469	344	74	112
Frame (fps)	1.3	2.1	2.9	13.6	8.9
Speedup	1×	1.7×	2.3×	9.6×	7×
Params (mils)	7.76	2.06	0.37	0.0039	0.0053
Param savings	1×	3.7×	21×	1990×	1464

TABLE III: Performance of MAVNet in comparison with other methods on NVIDIA Jetson Xavier. The input image is  $1024 \times 1280 \times 3$ . Mean IoU 1 is the average of IoU of classes on the penstock dataset. Mean IoU 2 is the average of IoU of classes on the penstock dataset. MAVNet features 400 less parameters than ErfNet while performing comparably on both datasets.

of this design is that the upsampling can reduce the refinement of the estimation, resulting in less accurate boundary prediction. This is shown in both Fig.7 and Fig. 8 as the areas predicted as corrosion and drone are usually larger than the ground truth. This issue can be solved by adding more layers between the two upsampling blocks but for most inspection and tracking tasks, this is unnecessary. Typically, the goal is to locate and identify instances of objects, not precisely bound their border.

## VIII. CONCLUSIONS

In this work, we proposed a data-efficient, data-driven image segmentation method using a fully convolutional neural network that can detect highly non-homogeneous objects under low-light and high-noise conditions fast on light, low power platforms.

Our method is extremely lightweight and can be seamlessly combined with other MAV planning algorithms to provide a completely automated and real-time inspection tool to replace humans in labor-intensive and dangerous tasks. Our approach can provide an automated solution for safer, faster, cost-efficient and objective infrastructure inspection.

We provide our datasets and implementation to encourage further research on MAV-based image segmentation problems.

## REFERENCES

- [1] E. Romera, J. M. Alvarez, L. M. Bergasa, and R. Arroyo, "Erfnet: Efficient residual factorized convnet for real-time semantic segmentation," *IEEE Transactions on Intelligent Transportation Systems*, vol. 19, no. 1, pp. 263–272, Jan 2018.
- [2] V. Kumar and N. Michael, "Opportunities and challenges with autonomous micro aerial vehicles," *The International Journal of Robotics Research*, vol. 31, no. 11, pp. 1279–1291, 2012.
- [3] T. Özaskan, G. Loianno, J. Keller, C. J. Taylor, and V. Kumar, "Spatio-temporally smooth local mapping and state estimation inside generalized cylinders with micro aerial vehicles," *IEEE Robotics and Automation Letters*, vol. 3, no. 4, pp. 4209–4216, Oct 2018.
- [4] Y. LeCun, Y. Bengio, and G. Hinton, "Deep learning," *nature*, vol. 521, no. 7553, p. 436, 2015.
- [5] L. Deng, D. Yu, *et al.*, "Deep learning: Methods and applications," *Foundations and Trends® in Signal Processing*, vol. 7, no. 3–4, pp. 197–387, 2014.
- [6] I. Sa, Z. Ge, F. Dayoub, B. Upcroft, T. Perez, and C. McCool, "Deepfruits: A fruit detection system using deep neural networks," *Sensors*, vol. 16, no. 8, p. 1222, 2016.

- [7] S. P. Mohanty, D. P. Hughes, and M. Salathé, "Using deep learning for image-based plant disease detection," *Frontiers in plant science*, vol. 7, p. 1419, 2016.
- [8] P. Sermanet, K. Kavukcuoglu, S. Chintala, and Y. LeCun, "Pedestrian detection with unsupervised multi-stage feature learning," in *Proceedings of the IEEE Conference on Computer Vision and Pattern Recognition*, 2013, pp. 3626–3633.
- [9] Y. Lv, Y. Duan, W. Kang, Z. Li, F.-Y. Wang, *et al.*, "Traffic flow prediction with big data: A deep learning approach," *IEEE Trans. Intelligent Transportation Systems*, vol. 16, no. 2, pp. 865–873, 2015.
- [10] Y.-J. Cha, W. Choi, and O. Büyüköztürk, "Deep learning-based crack damage detection using convolutional neural networks," *Computer-Aided Civil and Infrastructure Engineering*, vol. 32, no. 5, pp. 361–378, 2017.
- [11] C. M. Yeum and S. J. Dyke, "Vision-based automated crack detection for bridge inspection," *Computer-Aided Civil and Infrastructure Engineering*, vol. 30, no. 10, pp. 759–770, 2015.
- [12] K. Makantasis, E. Protopapadakis, A. Doulamis, N. Doulamis, and C. Loupos, "Deep convolutional neural networks for efficient vision based tunnel inspection," in *Intelligent Computer Communication and Processing (ICCP), 2015 IEEE International Conference on*. IEEE, 2015, pp. 335–342.
- [13] K. He, X. Zhang, S. Ren, and J. Sun, "Deep residual learning for image recognition," *2016 IEEE Conference on Computer Vision and Pattern Recognition (CVPR)*, Jun 2016. [Online]. Available: <http://dx.doi.org/10.1109/CVPR.2016.90>
- [14] M. Saska, "Mav-swarm: Unmanned aerial vehicles stabilized along a given path using onboard relative localization," in *2015 International Conference on Unmanned Aircraft Systems (ICUAS)*, June 2015, pp. 894–903.
- [15] D. Maturana, S. Arora, and S. Scherer, "Looking forward: A semantic mapping system for scouting with micro-aerial vehicles," in *2017 IEEE/RSJ International Conference on Intelligent Robots and Systems (IROS)*, Sep. 2017, pp. 6691–6698.
- [16] J. Rau, K. Hsiao, J. Jhan, S. Wang, W. Fang, and J. Wang, "Bridge crack detection using multi-rotary uav and object-base image analysis," *The International Archives of Photogrammetry, Remote Sensing and Spatial Information Sciences*, vol. 42, p. 311, 2017.
- [17] T. Özaskan, G. Loianno, J. Keller, C. J. Taylor, V. Kumar, J. M. Wozenraft, and T. Hood, "Autonomous navigation and mapping for inspection of penstocks and tunnels with mavs," *IEEE Robotics and Automation Letters*, vol. 2, no. 3, pp. 1740–1747, July 2017.
- [18] J. Hochstetler, R. Padidela, Q. Chen, Q. Yang, and S. Fu, "Embedded deep learning for vehicular edge computing," in *2018 IEEE/ACM Symposium on Edge Computing (SEC)*, Oct 2018, pp. 341–343.
- [19] A. Geiger, P. Lenz, and R. Urtasun, "Are we ready for autonomous driving? the kitti vision benchmark suite," in *Conference on Computer Vision and Pattern Recognition (CVPR)*, 2012.
- [20] M. Cordts, M. Omran, S. Ramos, T. Rehfeld, M. Enzweiler, R. Benenson, U. Franke, S. Roth, and B. Schiele, "The cityscapes dataset for semantic urban scene understanding," *2016 IEEE Conference on Computer Vision and Pattern Recognition (CVPR)*, Jun 2016. [Online]. Available: <http://dx.doi.org/10.1109/CVPR.2016.350>
- [21] K. Simonyan and A. Zisserman, "Very deep convolutional networks for large-scale image recognition," 2014.
- [22] A. Paszke, A. Chaurasia, S. Kim, and E. Cukurciello, "Enet: A deep neural network architecture for real-time semantic segmentation," *arXiv preprint arXiv:1606.02147*, 2016.
- [23] A. G. Howard, M. Zhu, B. Chen, D. Kalenichenko, W. Wang, T. Weyand, M. Andreetto, and H. Adam, "Mobilenets: Efficient convolutional neural networks for mobile vision applications," 2017.
- [24] A. C. L. S. Sachin Mehta, Mohammad Rastegari and H. Hajishirzi, "Espnet: Efficient spatial pyramid of dilated convolutions for semantic segmentation," in *ECCV*, 2018.
- [25] H. Zhao, X. Qi, X. Shen, J. Shi, and J. Jia, "Icnet for real-time semantic segmentation on high-resolution images," *Lecture Notes in Computer Science*, p. 418434, 2018. [Online]. Available: [http://dx.doi.org/10.1007/978-3-030-01219-9\\_25](http://dx.doi.org/10.1007/978-3-030-01219-9_25)
- [26] J.-K. Park, B.-K. Kwon, J.-H. Park, and D.-J. Kang, "Machine learning-based imaging system for surface defect inspection," *International Journal of Precision Engineering and Manufacturing-Green Technology*, vol. 3, no. 3, pp. 303–310, 2016.
- [27] T. Özaskan, G. Loianno, J. Keller, C. J. Taylor, V. Kumar, J. M. Wozenraft, and T. Hood, "Autonomous navigation and mapping for

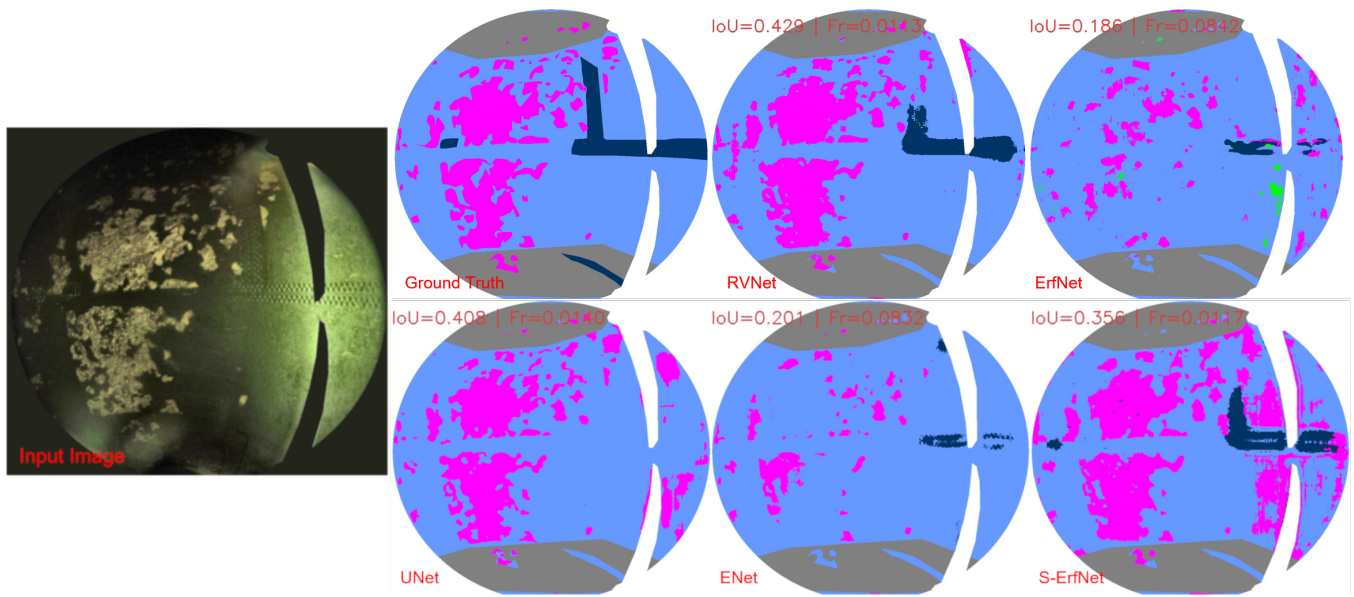


Fig. 7: Qualitative visualization showing the performance of networks on penstock dataset. IoU for corrosion for each network is shown. MAVNet outperforms the other methods on this sample.

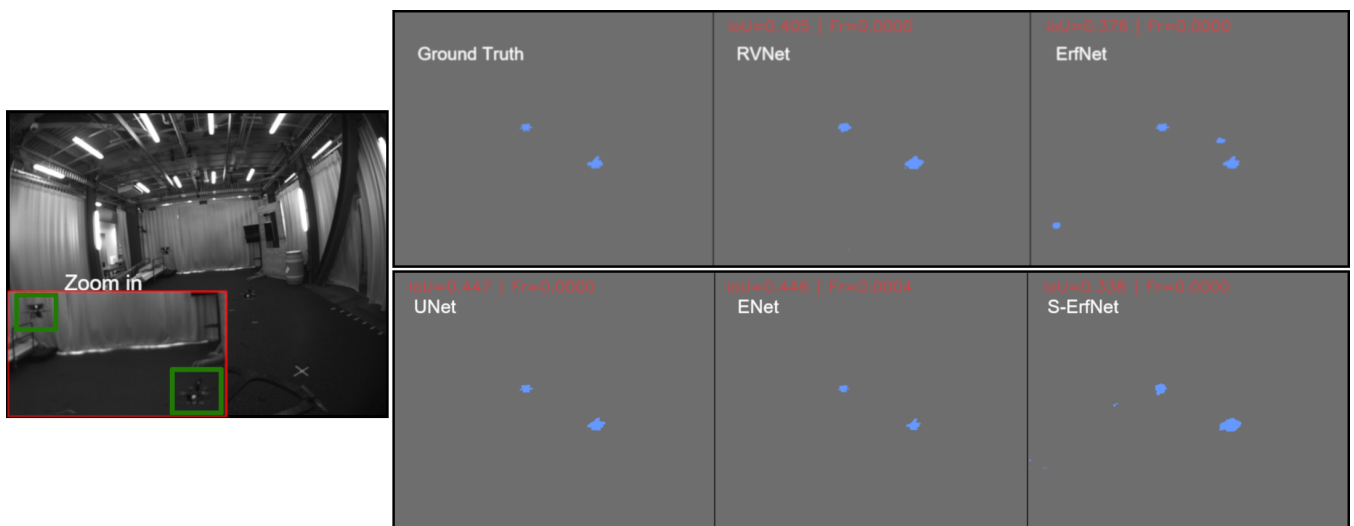


Fig. 8: Qualitative visualization showing the performance of networks on drone detection dataset. IoU for drone for each network is shown. MAVNet outperforms ErfNet, S-ErfNet and performs comparably to other methods.

inspection of penstocks and tunnels with mavs,” *IEEE Robotics and Automation Letters*, vol. 2, no. 3, pp. 1740–1747, 2017.

[28] M. Quigley, K. Mohta, S. S. Shivakumar, M. Watterson, Y. Mulgaonkar, M. Arguedas, K. Sun, S. Liu, B. Pfrommer, V. Kumar, *et al.*, “The open vision computer: An integrated sensing and compute system for mobile robots,” *arXiv preprint arXiv:1809.07674*, 2018.

[29] J. Long, E. Shelhamer, and T. Darrell, “Fully convolutional networks for semantic segmentation,” in *Proceedings of the IEEE conference on computer vision and pattern recognition*, 2015, pp. 3431–3440.

[30] O. Ronneberger, P. Fischer, and T. Brox, “U-net: Convolutional networks for biomedical image segmentation,” in *International Conference on Medical image computing and computer-assisted intervention*. Springer, 2015, pp. 234–241.

[31] V. Badrinarayanan, A. Kendall, and R. Cipolla, “Segnet: A deep convolutional encoder-decoder architecture for image segmentation,” *IEEE transactions on pattern analysis and machine intelligence*, vol. 39, no. 12, pp. 2481–2495, 2017.

[32] K. Simonyan and A. Zisserman, “Very deep convolutional networks for large-scale image recognition,” *arXiv preprint arXiv:1409.1556*, 2014.

[33] L.-C. Chen, Y. Zhu, G. Papandreou, F. Schroff, and H. Adam, “Encoder-decoder with atrous separable convolution for semantic image segmentation,” in *Proceedings of the European Conference on Computer Vision (ECCV)*, 2018, pp. 801–818.

[34] T.-Y. Lin, P. Goyal, R. Girshick, K. He, and P. Dollár, “Focal loss for dense object detection,” *IEEE transactions on pattern analysis and machine intelligence*, 2018.

[35] M. Abadi, P. Barham, J. Chen, Z. Chen, A. Davis, J. Dean, M. Devin, S. Ghemawat, G. Irving, M. Isard, *et al.*, “Tensorflow: a system for large-scale machine learning,” in *OSDI*, vol. 16, 2016, pp. 265–283.

[36] D. P. Kingma and J. Ba, “Adam: A method for stochastic optimization,” *arXiv preprint arXiv:1412.6980*, 2014.